Nano Research
DOI 10.1007/s12274-014-0594-9
Research Article
ISSN 1998-0124
CN 11-5974/O4

Electrical field tuning of magneto-Raman scattering in monolayer graphene

Xiaonan Shen[1,§], Caiyu Qiu[1,2,§], Bingchen Cao[1], Chunxiao Cong[1], Weihuang Yang[1], Haomin Wang[1], and Ting Yu[1,3,4] (✉)

[1] *Division of Physics and Applied Physics, School of Physical and Mathematical Sciences, Nanyang Technological University, 637371 Singapore, Singapore*
[2] *Wenzhou Institute of Biomaterials and Engineering, Wenzhou 325001, China*
[3] *Department of Physics, Faculty of Science, National University of Singapore, 117542 Singapore, Singapore*
[4] *Graphene Research Center, Faculty of Science, National University of Singapore, 117546 Singapore, Singapore*
§ *These authors contributed equally to this work.*

Received: 6 June 2014
Revised: 17 September 2014
Accepted: 24 September 2014

KEYWORDS
monolayer graphene,
magneto-phonon resonance,
Raman,
electrical field,
suspended graphene

ABSTRACT

In this work, we report the electrical field tuning of magneto-phonon resonance in monolayer graphene under magnetic fields up to 9 T. It is found that the carrier concentration can drastically affect the G (E_{2g}) phonon response to a varying magnetic field through a pronounced magneto-phonon resonance (MPR). In charge neutral or slightly doped monolayer graphene, both the energy and the line width of the E_{2g} phonon show clear variation with magnetic fields. This is attributed to magneto-phonon resonance between magnetoexcitations and the E_{2g} phonons. In contrast, when the Fermi level of the monolayer graphene is far away from the Dirac point, the G band shows weak magnetic dependence and exhibits a symmetric line-shape. This suggests that the magneto-phonon coupling around 4 T has been switched off due to the Pauli blocking of the inter-Landau level excitations. Moreover, the G band asymmetry caused by Fano resonance between excitonic many-body states and the E_{2g} phonons is observed. This work offers a way to study the magnetoexcitation phonon interaction of materials through magneto-Raman spectroscopy with an external electrical field.

1 Introduction

The magneto-phonon resonance (MPR) effect has been investigated in a variety of two-dimensional systems [1–9] and predicted to exist in graphene-related systems. For example, the G phonon in monolayer

Address correspondence to yuting@ntu.edu.sg

graphene would show magnetic field dependent variation due to the coupling to the electronic magnetoexcitations [10, 11]. Especially, the inter-Landau-level (LL) electronic transitions $LL^{-1,2}_{-2,1}$ and $LL^{0,1}_{-1,0}$ are expected to have strong coupling with the G phonons at about 5 and 30 T [11], respectively. Here, $LL^{-n,n+1}_{-n-1,n}$ stands for the inter-LL transitions both from L_{-n-1} to L_n and from L_{-n} to L_{n+1} (L_n represents the LL with an index of n, where $n = 0, 1, 2\ldots$). Raman spectroscopy is a widely employed technique to study various properties of graphene [12–21]. Recently, the MPR effect in graphene-related systems was observed through magneto-Raman spectroscopy (Raman spectroscopy in a magnetic field) by several groups [22–26], where the G phonons exhibit a clear magnetic dependent variation. The Fermi level or filling factor was anticipated and observed to greatly affect the MPR effect in monolayer graphene [7–10]. Potemski's work observed the magneto-phonon effect due to the coupling between the G phonons and LL^{0}_{-1} in mechanically exfoliated monolayer graphene [7]. From their results, the sample was identified to be p-type doped and the filling factor value is between 2 and 6 at about 25 T. However, this work only studied accidentally doped graphene samples with carrier concentrations typical for graphene deposited on Si/SiO_2 substrates. Kim et al. studied the MPR in adsorption-doped CVD-grown monolayer graphene samples [8]. The different doping levels were obtained by adjusting annealing parameters and by exposure to ambient pressure N_2 gas or air, which is not very tunable compared to electrically gated graphene in the sense of uniformity or control. Very recently, a comprehensive study of the electrical tuning of the fundamental MPR induced by $LL^{-1,0}_{0,1}$ excitations in CVD grown graphene has been reported [9]. The measurements were conducted at extremely high constant magnetic fields around 25 T while sweeping the gate voltage. However, a study of the effect of relatively high doping levels on MPR under a relatively low magnetic field is still missing and the topic needs to be investigated.

Here, we report a study on the MPR effect involving $LL^{-1,2}_{-2,1}$ in an electrically tuned monolayer graphene by magneto-Raman experiments. The carrier concentration in the sample was tuned by a back gate, so that the filling factor of LL under a magnetic field was altered accordingly. Consequently, responses of the G phonons of monolayer graphene to the magnetic field with different gate voltages reflect the filling factor effect on MPR. By tuning the Fermi level to reach zero/large filling factors, we clearly show that the MPR effect can be switched on/off in magnetic fields around 4 T. Suspended exfoliated monolayer graphene, which is newly studied, presents an obvious MPR effect. In addition, an asymmetric line-shape of the Raman G band is observed in electrically neutral graphene at low temperature and interpreted in terms of Fano resonance.

2 Experimental

Graphene samples were prepared by mechanical exfoliation from natural graphite crystals and transferred onto a 300 nm SiO_2/Si substrate [27]. Monolayer graphene flakes were identified by using both optical contrast spectroscopy and Raman spectroscopy [28, 29]. Electron beam lithography was utilized to define the geometry of electrodes [30], and then Ti (5 nm)/Au (60 nm) were deposited to form contact electrodes. The electron and hole mobilities can be extracted from the transport data and the values are about 9,490 and 8,050 $cm^2 \cdot V^{-1} \cdot s^{-1}$, respectively (Fig. S4 in the Electronic Supplementary Material (ESM)).

The low-temperature magneto-Raman measurements were performed in a cryostat with a custom designed confocal micro-Raman spectroscopy/image system (see Fig. 1(a)). A linearly polarized incident laser (Nd:YAG, 532 nm) with a ~1 μm beam size and a power less than 5 mW was used to illuminate the sample. The diameters of the optical fibers for delivering the laser and collecting signal were 5 and 50 μm, respectively. Similar to our previous experimental setup [25], both co-circular and cross-circular polarized signals can be simultaneously collected. Perpendicular magnetic fields of up to 9 T were generated by a superconductor magnet mounted inside the cryostat. A Keithley 4200 semiconductor characterization system was used to measure the electrical response of the graphene device and to provide a fixed gate voltage.

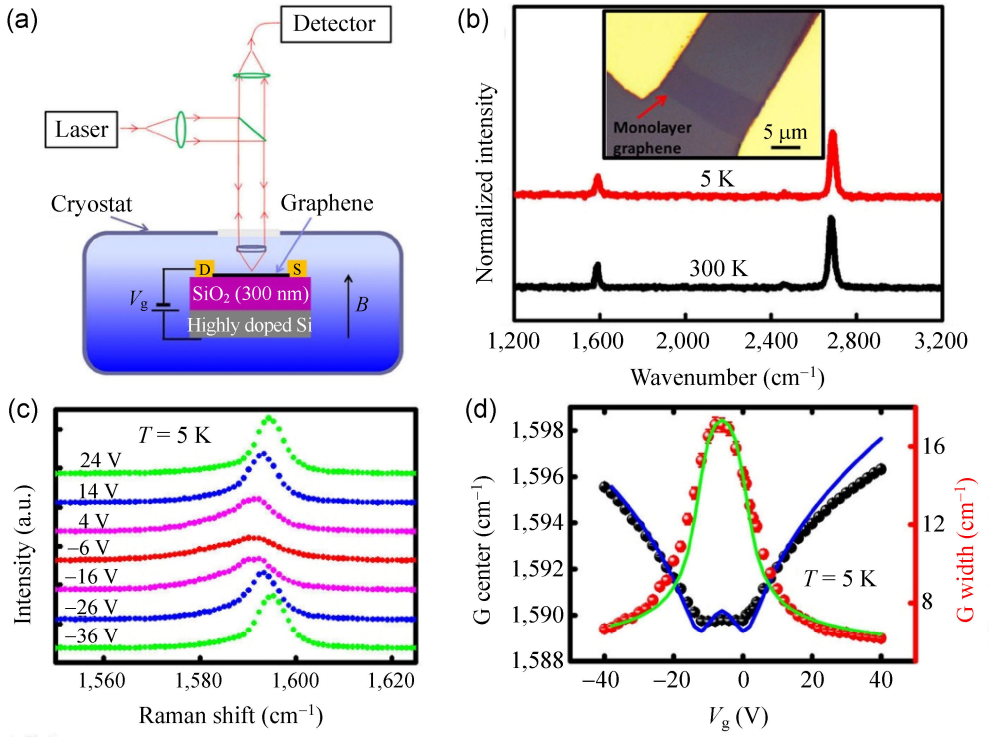

Figure 1 (a) A schematic for the experimental setup for the magneto-Raman measurements. (b) Raman spectra on monolayer graphene at room temperature (~300 K, black curve) and low temperature (~5 K, red curve). Inset is optical image of the graphene device. (c) Raman spectra of a graphene device under various gate voltages at 5 K. The red curve (V_g = –6 V) corresponds to the case when the Fermi level is brought near to the Dirac point. (d) Positions (black spheres) and widths (red spheres) of the G peak as a function of the gate voltage. Simulation results are shown in blue and green lines.

3 Results and discussion

Raman spectra of the monolayer graphene device are shown in Fig. 1(b). The Raman D peak which is located around 1,350 cm^{-1} is undetectable, indicating the high quality of the sample. To tune the doping level, it is necessary to know the charge neutral point (NP, also known as the Dirac point) of the graphene sample [31]. We prefer to use gated Raman measurements rather than electrical transport measurements to examine the NP value since Raman spectroscopy can reflect the local properties. Gated Raman measurements were performed (at ~ 5 K) by sweeping the gate voltage (V_g) from –40 to 40 V and selected spectra are shown in Fig. 1(c). The frequency and full width at half maximum (FWHM) of the G band as a function of gate voltage were extracted by fitting each peak into a single Lorentzian peak and are plotted in Fig. 1(d). Softened G phonons can be observed at the charge neutral Dirac point due to the Kohn anomaly [13, 18] and hence the NP of the sample can be determined to be at –6 V.

Magneto-Raman spectra of the monolayer graphene when V_g = –6 and 24 V are shown in Figs. 2(a) and 2(b), respectively. In these spectra, the G bands show a single peak profile with no obvious G peak split. However, when V_g is –6 V, asymmetric broadening on the lower frequency side of the G band can be observed (see Fig. 2(c)). G peak asymmetry/splitting has also been previously observed and was attributed to the circular dichroism effect occurring only under a high magnetic field [7, 32]. However, our measured Raman G peak shows maximum asymmetry at a zero magnetic field. Thus, the asymmetric line shape presented here is most probably due to other reasons. Fano resonance between the renormalized phonon excitation and a continuum of excitonic many-body states, therefore, could be responsible and the peaks can be fitted by the Breit–Wigner–Fano (BWF) line shape [33, 34]

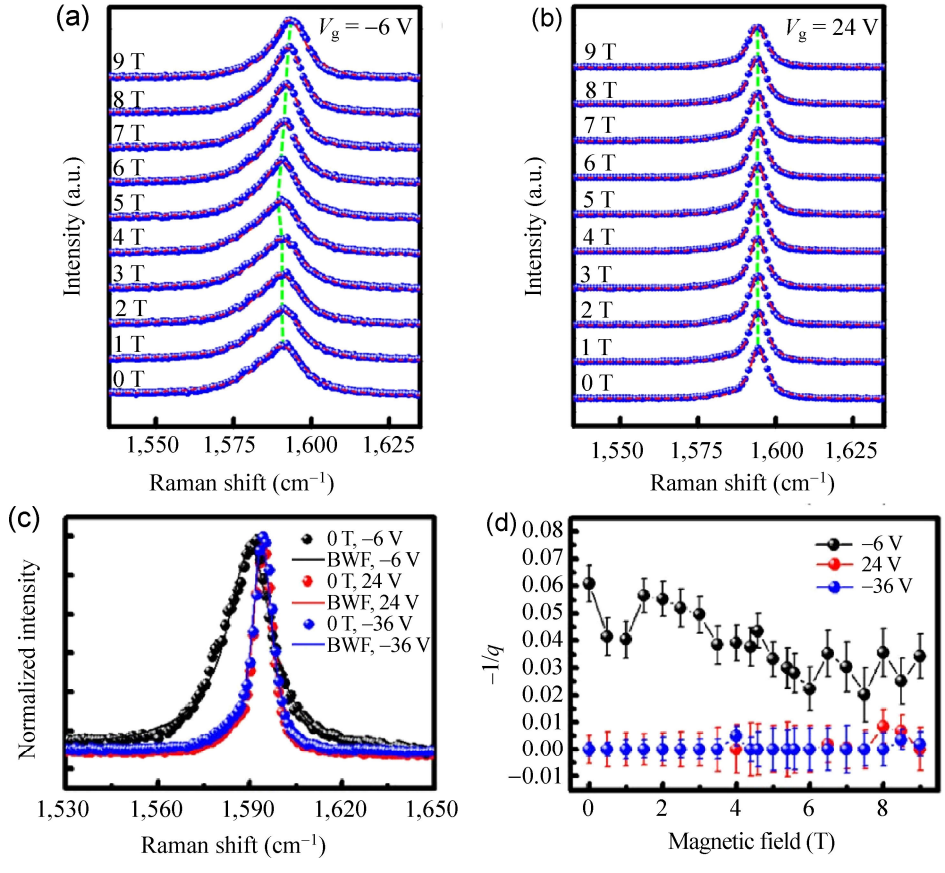

Figure 2 Raman spectra of monolayer graphene at different magnetic fields measured at low temperature (~ 5 K) with back gate voltages of (a) V_g = –6 and (b) 24 V applied. Blue spheres represent raw data and the red dashed lines are the fitting curves. Green dashed lines are a guide to the eyes. (c) Comparison of the G peak line shapes for a graphene sample in the cases of the neutral point (V_g = –6 V) and electrically doped (V_g = 24 V; V_g = –36 V). The solid lines are obtained by fitting the data points to the BWF line shape using Eq. (1). (d) The summarized asymmetry factor –1/q for the Raman spectra recorded under these three gate voltages.

$$I(\omega) = I_0 \frac{[1+2(\omega-\omega_0)/(q\Gamma)]^2}{[1+4(\omega-\omega_0)^2/\Gamma^2]} \quad (1)$$

where $1/|q|$ is the asymmetry factor or coupling coefficient, and I_0, ω_0, and Γ are the intensity, uncoupled BWF peak frequency and broadening parameter, respectively. In the limit $q \to \infty$, the line shape is symmetric and shows the standard Lorentzian profile, indicating a weak interference or coupling. The extracted values for –1/q under various gate voltages (see Fig. S5, in the ESM) are comparable to previous work by Yoon et al. [33]. Both sets of –1/q data are within the range of 0.08 to 0, and vanish when the Fermi energy is sufficiently large (~0.2 eV for both our sample and Yoon's sample). When the graphene is either electron or hole doped to a certain extent, the values of –1/q are around 0. The absence of Fano resonance in doped graphene is consistent with a previous report and is attributed to the suppressed excitonic processes [33]. The fitted –1/q values as a function of magnetic field under three different gate voltages are summarized in Fig. 2(d). When the Fermi level of graphene is tuned to be near Dirac point, the –1/q values are all non-zero and show a maximum value at 0 T. The presence of a magnetic field splits the continuum band structure of graphene into discrete Landau levels, thereby weakening Fano resonance as the magnetic field increases. A similar modification of Fano resonance by magnetic fields has been reported in quantum wells [35, 36]. Note that the Fano resonance is not considered to be an important factor affecting the MPR effect in this work.

The evolution of the frequency and the FWHM of the G peak for the monolayer graphene with magnetic field at three different gate voltages are shown in Figs. 3(a) and 3(b), respectively. As shown in Fig. 3(a),

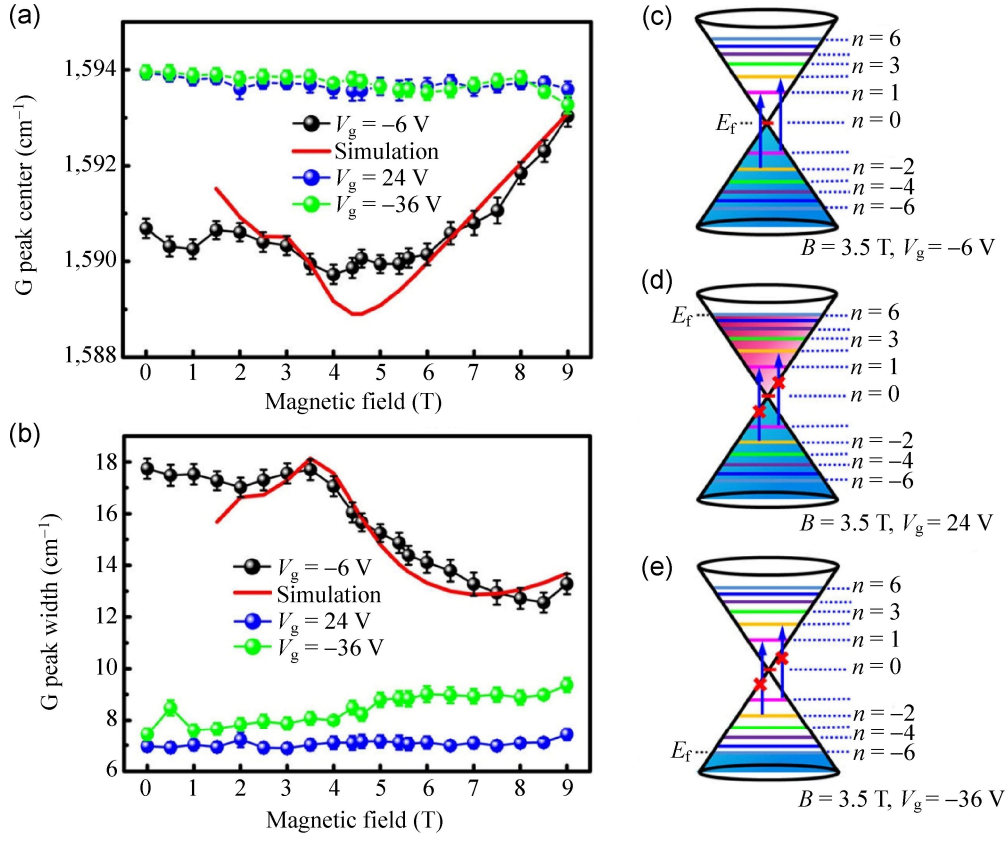

Figure 3 The evolutions of (a) the BWF peak frequency and (b) the width of the G peak for the monolayer graphene with magnetic field under different gate voltages. V_g values are –6, 24 and –36 V for black, blue and green curves, respectively. Simulation results are also shown. Schematic images for different doping situations in monolayer graphene when different back gate voltages are applied at B = 3.5 T. Discrete LLs are labeled with corresponding LL indexes. Fermi levels in these cases are also indicated. Vertical blue lines indicate the inter-LL transitions. (c) V_g = –6 V. The indicated inter-LL transitions are possible in this case. (d) V_g = 24 V. The indicated inter-LL transitions are suppressed in this case. (e) V_g = –36 V. The indicated inter-LL transitions are suppressed in this case.

it is clear that the frequency of the G phonons shows a magnetic field dependent variation when V_g is –6 V. In detail, the G band frequency decreases (with fluctuations) before reaching its minimum value of about 1,589.5 cm^{-1} at about 4 T. After this point, it keeps rising to its maximum value of about 1,593.0 cm^{-1} at 9 T. For the FWHM values shown in Fig. 3(b), the maximum is located at about 3.5 T and then the FWHM value decreases with further increases in the magnetic field. In contrast, both the frequency and the FWHM of the G peak show weak magnetic dependence when the sample is highly n-type or p-type doped.

The results shown in Fig. 3 can be well interpreted by the MPR theory. Discrete LLs appear when the graphene is subjected to a magnetic field. The energy of the LL with an index of n (E_n) is proportional to the square root of the index n and the magnetic field strength B [37, 38]

$$E_n = \mathrm{sgn}(n)\sqrt{2e\hbar v_F^{\,2}B|n|} \quad (1)$$

where v_F is the Fermi velocity, and n>0 and n<0 represent electrons and holes, respectively. The energy of the inter-LL electronic excitations for $LL^{-n,n+1}_{-n-1,n}$ (which is denoted by $E^{-n,n+1}_{-n-1,n}$ here) is

$$E^{-n,n+1}_{-n-1,n} = (\sqrt{n+1}+\sqrt{n})\sqrt{2e\hbar V_F^{\,2}B} \quad (2)$$

MPR occurs when the energy of the inter-LL transitions is equal to the E_{2g} phonon energy at a certain B field (i.e. the resonant magnetic field), which leads to magnetic oscillation of the G-band phonons. According to Ando's calculations, the spectral width will become a maximum and the frequency will changing rapidly

at the resonant B field [10]. We therefore deduce that MPR occurs at about 3.5 T and is associated with the $LL^{-1,2}_{-2,1}$ transition according to our experimental data. Considering the MPR condition of $E^{-1,2}_{-2,1}$ = 196.8 meV (the G phonon energy is ~ 196.8 meV at 5 K without a magnetic field), the Fermi velocity v_F of the sample can be calculated to be about 1.21×10^6 $m^2 \cdot s^{-1}$. This v_F value is reasonable [39, 40] and agrees well with the values given in other reports for monolayer graphene [37, 38, 41]. We also carried out simulations using the same model as in Potemski's work [42] (see details in the ESM), and extracted the following parameters: The interaction parameter $\lambda = 5 \times 10^{-3}$, the broadening factor $\delta = 400$ $cm^{-1} = 49.6$ meV, the phonon energy at zero magnetic field $\varepsilon_0 = 1,586.6$ cm^{-1}, and the Fermi velocity $v_F = 1.21 \times 10^6$ $m^2 \cdot s^{-1}$. These values are comparable to earlier reports [7, 26, 32, 42]. Furthermore, substituting these values in Ando's model for the phonon anomaly phenomenon (see details in the ESM) at B = 0 T [32], the experimental data can be fairly well reproduced as shown in Fig. 1(d).

Now we would like to discuss the doping effect on MPR in the monolayer graphene sample. When a V_g of –6 V was applied to the sample, its filling factor υ is around 0. In this case, only the central LL (n = 0) is half filled. Thus, inter-LL electronic excitations $LL^{-1,2}_{-2,1}$ are allowed and can couple to the G phonon. Both high level p-type and n-type doping, which yield large filling factors, can block the inter-LL electronic excitations and thus suppress MPR effect in graphene. The filling factor in monolayer graphene can be calculated [41, 43, 44]

$$\upsilon = \frac{n_s}{eB/h}$$
$$n_s = C_g \left| V_g - V_{Dirac} \right| / e \quad (3)$$
$$\upsilon = g_s (n + 1/2)$$

where υ is the filling factor and n_s is the carrier density. $g_s = 4$, accounting for the spin degeneracy and sublattice degeneracy. C_g denotes the gate capacitance and is ~115 $aF \cdot \mu m^{-2}$. Based on Eq. (3), the filling factor in our sample is υ = 26 under a field of B = 3.5 T when V_g = 24 V/–36 V, which means that the electrons will fill to the LL with index $n = \pm 6$. Schematic images for these three different doping situations (B = 3.5 T) in monolayer graphene are shown in Figs. 3(c)–3(e). Consequently, the inter-LL excitations $LL^{-1,2}_{-2,1}$ become inactive in both cases resulting in the suppression of their hybridization with the G phonon.

The MPR effect in several as-prepared mechanically exfoliated supported and suspended monolayer graphene samples was also investigated. Here we should mention that weak residual strains (less than 1%) may exist in the samples after cooling to low temperatures [16]. The interpretation of the data is not be affected, however, because the weak strain should not significantly affect the MPR [9, 45]. The results for a suspended monolayer graphene are displayed in Fig. 4. There are more than ten suspended regions in this graphene sample (Fig. 4(a)) and distinct magnetic field dependent variations of the frequency and the FWHM of the G peak can be observed from all randomly measured regions. The results shown in Fig. 4(b) are obtained from the region numbered 5 and

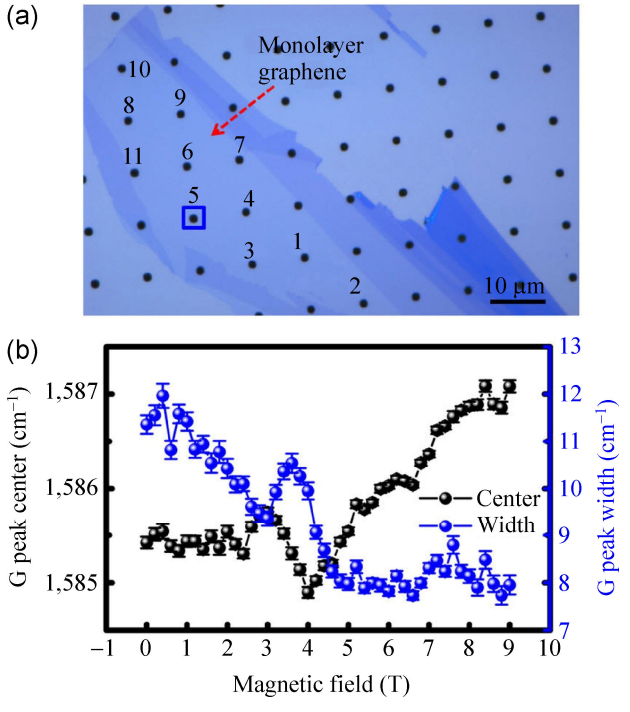

Figure 4 (a) Optical image of the as exfoliated sample on a substrate with patterned holes. More than 10 holes on the substrate were covered by this monolayer graphene (indicated by the red arrow, holes are numbered to identify different suspended graphene areas). The diameter of a hole is about 3 μm while the laser spot size is about 1 μm. (b) G peak center (black spheres) and width (blue spheres) as a function of magnetic field for the suspended monolayer graphene region numbered 5 (indicated by the blue square).

the resonant field is about 3.6 T. Notice that the oscillation in the suspended sample is the most obvious among all the graphene samples studied in this work. Comparing the widths of their G bands (Figs. 3(b) and 4(b)), we can see that the suspended graphene sample possesses a narrower G band than the supported graphene, suggesting a longer phonon lifetime. We suspect that the longer phonon lifetime in the sample represents a higher quality, which is an important factor affecting the MPR in graphene [46]. Due to the elimination of both the substrate effect and the influence caused by device fabrication, the suspended graphene can have the longest lifetime of all these samples. This assumption can be further confirmed by the fact that the graphene-like region on the graphite substrate with a much narrower G peak width of ~4 cm^{-1} shows a more prominent MPR effect than other graphene samples [22, 25].

4 Conclusions

We have reported magneto-Raman results obtained by sweeping relatively low magnetic fields in mechanically exfoliated monolayer graphene under different situations: (1) Fabricated as field-effect devices and electrically tuned to fixed doping levels; (2) supported on SiO_2/Si; (3) suspended from the substrate. The MPR effect involving $LL^{-1,2}_{-2,1}$ transitions appears when the filling factor is near zero, and disappears when the sample is highly doped due to Pauli blocking. A filling factor effect on MPR in monolayer graphene is thus experimentally observed and matches well with theoretical predictions. This is the first reported MPR study of suspended samples and the fact that they show the clearest oscillations of all the studied samples indicates the importance of sample quality. In addition, Fano resonance is proposed to explain the observed asymmetric line shape of the Raman G band in electrically neutral graphene. Furthermore, the magnetic field effect on the Fano resonance has been demonstrated in our work. A detailed understanding of the magnetic field induced modification of Fano resonance in graphene and other 2D materials could be useful in future work. These findings extend our knowledge of MPR in graphene and may trigger pertinent theoretical studies. We believe that the findings here will be of interest to the graphene and other 2D system research communities.

Acknowledgement

This work is supported by the Singapore National Research Foundation under NRF RF award (No. NRF-RF2010-07) and MOE Tier 2 (No. MOE2012-T2-2-049). We thank Jeil Jung, Penghui Yao and Jingzhi Shang for their helpful discussion.

Electronic Supplementary Material: Supplementary material (calibration test for the custom designed magneto-Raman system, magneto-Raman scattering study on supported monolayer graphene, simulations for monolayer graphene, mobility of the carriers in the graphene device, phonon anomalies in the graphene device and Fano resonance in the graphene device) is available in the online version of this article at http://dx.doi.org/10.1007/s12274-014-0594-9.

References

[1] Barnes, D. J.; Nicholas, R. J.; Peeters, F. M.; Wu, X. G.; Devreese, J. T.; Singleton, J.; Langerak, C. J. G. M.; Harris, J. J.; Foxon, C. T. Observation of optically detected magnetophonon resonance. *Phys. Rev. Lett.* **1991**, *66*, 794–797.

[2] Vaughan, T. A.; Nicholas, R. J.; Langerak, C. J. G. M.; Murdin, B. N.; Pidgeon, C. R.; Mason, N. J.; Walker, P. J. Direct observation of magnetophonon resonances in Landau-level lifetimes of a semiconductor heterostructure. *Phys. Rev. B* **1996**, *53*, 16481–16484.

[3] Nicholas, R. J. The magnetophonon effect. *Prog. Quantum Electron.* **1985**, *10*, 1–75.

[4] Firsov, Y. A.; Gurevich, V. L.; Parfeniev, R. V.; Shalyt, S. S. Investigation of a new type of oscillations in the magnetoresistance. *Phys. Rev. Lett.* **1964**, *12*, 660–662.

[5] Tsui, D. C.; Englert, T.; Cho, A. Y.; Gossard, A. C. Observation of magnetophonon resonances in a two-dimensional electronic system. *Phys. Rev. Lett.* **1980**, *44*, 341–344.

[6] Stradling, R. A.; Wood, R. A. The magnetophonon effect in III-V semiconducting compounds. *J. Phys. C: Solid State Phys.* **1968**, *1*, 1711.

[7] Kossacki, P.; Faugeras, C.; Kühne, M.; Orlita, M.; Mahmood, A.; Dujardin, E.; Nair, R. R.; Geim, A. K.; Potemski, M. Circular dichroism of magnetophonon resonance in doped graphene. *Phys. Rev. B* **2012**, *86*, 205431.

[8] Kim, Y.; Poumirol, J. M.; Lombardo, A.; Kalugin, N. G.; Georgiou, T.; Kim, Y. J.; Novoselov, K. S.; Ferrari, A. C.; Kono, J.; Kashuba, O. et al. Measurement of filling-factor-dependent magnetophonon resonances in graphene using raman spectroscopy. *Phys. Rev. Lett.* **2013**, *110*, 227402.

[9] Leszczynski, P.; Han, Z.; Nicolet, A. A. L.; Piot, B. A.; Kossacki, P.; Orlita, M.; Bouchiat, V.; Basko, D. M.; Potemski, M.; Faugeras, C. Electrical switch to the resonant magneto-phonon effect in graphene. *Nano Lett.* **2014**, *14*, 1460–1466.

[10] Ando, T. Magnetic oscillation of optical phonon in graphene. *J. Phys. Soc. Jpn.* **2007**, *76*, 024712.

[11] Goerbig, M. O.; Fuchs, J. N.; Kechedzhi, K.; Fal'ko, V. I. Filling-factor-dependent magnetophonon resonance in graphene. *Phys. Rev. Lett.* **2007**, *99*, 087402.

[12] Das, A.; Pisana, S.; Chakraborty, B.; Piscanec, S.; Saha, S. K.; Waghmare, U. V.; Novoselov, K. S.; Krishnamurthy, H. R.; Geim, A. K.; Ferrari, A. C. et al. Monitoring dopants by Raman scattering in an electrochemically top-gated graphene transistor. *Nat. Nanotechnol.* **2008**, *3*, 210–215.

[13] Yan, J.; Zhang, Y.; Kim, P.; Pinczuk, A. Electric field effect tuning of electron-phonon coupling in graphene. *Phys. Rev. Lett.* **2007**, *98*, 166802.

[14] Luo, Z. Q.; Yu, T.; Ni, Z. H.; Lim, S. H.; Hu, H. L.; Shang, J. Z.; Liu, L.; Shen, Z. X.; Lin, J. Y. Electronic structures and structural evolution of hydrogenated graphene probed by Raman spectroscopy. *J. Phys. Chem. C* **2011**, *115*, 1422–1427.

[15] Luo, Z. Q.; Yu, T.; Kim, K. J.; Ni, Z. H.; You, Y. M.; Lim, S. H.; Shen, Z. X.; Wang, S. Z.; Lin, J. Y. Thickness-dependent reversible hydrogenation of graphene layers. *ACS Nano* **2009**, *3*, 1781–1788.

[16] Ni, Z. H.; Yu, T.; Lu, Y. H.; Wang, Y. Y.; Feng, Y. P.; Shen, Z. X. Uniaxial strain on graphene: Raman spectroscopy study and band-gap opening. *ACS Nano* **2008**, *2*, 2301–2305.

[17] Yu, T.; Ni, Z. H.; Du, C. L.; You, Y. M.; Wang, Y. Y.; Shen, Z. X. Raman mapping investigation of graphene on transparent flexible substrate: The strain effect. *J. Phys. Chem. C* **2008**, *112*, 12602–12605.

[18] Malard, L. M.; Pimenta, M. A.; Dresselhaus, G.; Dresselhaus, M. S. Raman spectroscopy in graphene. *Phys. Rep.* **2009**, *473*, 51–87.

[19] Cong, C.; Yu, T.; Saito, R.; Dresselhaus, G. F.; Dresselhaus, M. S. Second-order overtone and combination Raman modes of graphene layers in the range of 1690–2150 cm^{-1}. *ACS Nano* **2011**, *5*, 1600–1605.

[20] Cong, C. X.; Yu, T.; Sato, K.; Shang, J. Z.; Saito, R.; Dresselhaus, G. F.; Dresselhaus, M. S. Raman characterization of ABA- and ABC-stacked trilayer graphene. *ACS Nano* **2011**, *5*, 8760–8768.

[21] Cong, C. X.; Yu, T.; Wang, H. M. Raman study on the G mode of graphene for determination of edge orientation. *ACS Nano* **2010**, *4*, 3175–3180.

[22] Yan, J.; Goler, S.; Rhone, T. D.; Han, M.; He, R.; Kim, P.; Pellegrini, V.; Pinczuk, A. Observation of magnetophonon resonance of Dirac fermions in graphite. *Phys. Rev. Lett.* **2010**, *105*, 227401.

[23] Faugeras, C.; Amado, M.; Kossacki, P.; Orlita, M.; Kühne, M.; Nicolet, A. A. L.; Latyshev, Y. I; Potemski, M. Magneto-Raman scattering of graphene on graphite: Electronic and phonon excitations. *Phys. Rev. Lett.* **2011**, *107*, 036807.

[24] Kühne, M.; Faugeras, C.; Kossacki, P.; Nicolet, A. A. L.; Orlita, M.; Latyshev, Y. I.; Potemski, M. Polarization-resolved magneto-Raman scattering of graphenelike domains on natural graphite. *Phys. Rev. B* **2012**, *85*, 195406.

[25] Qiu, C. Y.; Shen, X. N.; Cao, B. C.; Cong, C. X.; Saito, R.; Yu, J. J.; Dresselhaus, M. S.; Yu, T. Strong magnetophonon resonance induced triple G-mode splitting in graphene on graphite probed by micromagneto Raman spectroscopy. *Phys. Rev. B* **2013**, *88*, 165407.

[26] Faugeras, C.; Kossacki, P.; Nicolet, A. A. L.; Orlita, M.; Potemski, M.; Mahmood, A.; Basko, D. M. Probing the band structure of quadri-layer graphene with magneto-phonon resonance. *New J. Phys.* **2012**, *14*, 095007.

[27] Novoselov, K. S.; Geim, A. K.; Morozov, S. V.; Jiang, D.; Zhang, Y.; Dubonos, S. V.; Grigorieva, I. V.; Firsov, A. A. Electric field effect in atomically thin carbon films. *Science* **2004**, *306*, 666–669.

[28] Ferrari, A. C.; Meyer, J. C.; Scardaci, V.; Casiraghi, C.; Lazzeri, M.; Mauri, F.; Piscanec, S.; Jiang, D.; Novoselov, K. S.; Roth, S.; Geim, A. K. Raman spectrum of graphene and graphene layers. *Phys. Rev. Lett.* **2006**, *97*, 187401.

[29] Ni, Z. H.; Wang, H. M.; Kasim, J.; Fan, H. M.; Yu, T.; Wu, Y. H.; Feng, Y. P.; Shen, Z. X. Graphene thickness determination using reflection and contrast spectroscopy. *Nano Lett.* **2007**, *7*, 2758–2763.

[30] Shen, X. N.; Wang, H. M.; Yu, T. How do the electron beam writing and metal deposition affect the properties of graphene during device fabrication? *Nanoscale* **2013**, *5*, 3352–3358.

[31] Sarma, S. D.; Adam, S.; Hwang, E. H.; Rossi, E. Electronic transport in two-dimensional graphene. *Rev. Mod. Phys.* **2011**, *83*, 407–470.

[32] Rémi, S.; Goldberg, B. B.; Swan, A. K. Charge tuning of nonresonant magnetoexciton phonon interactions in graphene. *Phys. Rev. Lett.* **2014**, *112*, 056803.

[33] Yoon, D.; Jeong, D.; Lee, H. J.; Saito, R.; Son, Y. W.; Lee, H. C.; Cheong, H. Fano resonance in Raman scattering of

graphene. *Carbon* **2013**, *61*, 373–378.

[34] Tan, P. H.; Han, W. P.; Zhao, W. J.; Wu, Z. H.; Chang, K.; Wang, H.; Wang, Y. F.; Bonini, N.; Marzari, N.; Pugno, N. et al. The shear mode of multilayer graphene. *Nat. Mater.* **2012**, *11*, 294–300.

[35] Oberli, D. Y.; Böhm, G.; Weimann, G.; Brum, J. A. Fano resonances in the excitation spectra of semiconductor quantum wells. *Phys. Rev. B* **1994**, *49*, 5757–5760.

[36] Bellani, V.; Pérez, E.; Zimmermann, S.; Viña, L.; Hey, R.; Ploog, K. Evolution of Fano resonances in two- and three-dimensional semiconductors with a magnetic field. *Solid State Commun.* **1996**, *97*, 459–464.

[37] Jiang, Z.; Henriksen, E. A.; Tung, L. C.; Wang, Y. J.; Schwartz, M. E.; Han, M. Y.; Kim, P.; Stormer, H. L. Infrared spectroscopy of Landau levels of graphene. *Phys. Rev. Lett.* **2007**, *98*, 197403.

[38] Jung, S.; Rutter, G. M.; Klimov, N. N.; Newell, D. B.; Calizo, I.; Hight-Walker, A. R.; Zhitenev, N. B.; Stroscio, J. A. Evolution of microscopic localization in graphene in a magnetic field from scattering resonances to quantum dots. *Nat. Phys.* **2011**, *7*, 245–251.

[39] Elias, D. C.; Gorbachev, R. V.; Mayorov, A. S.; Morozov, S. V.; Zhukov, A. A.; Blake, P.; Ponomarenko, L. A.; Grigorieva, I. V.; Novoselov, K. S.; Guinea, F. et al. Dirac cones reshaped by interaction effects in suspended graphene. *Nat. Phys.* **2011**, *7*, 701–704.

[40] Hwang, C.; Siegel, D. A.; Mo, S. K.; Regan, W.; Ismach, A.; Zhang, Y. G.; Zettl, A.; Lanzara, A. Fermi velocity engineering in graphene by substrate modification. *Sci. Rep.* **2012**, *2*, 590.

[41] Zhang, Y. B.; Tan, Y. W.; Stormer, H. L.; Kim, P. Experimental observation of the quantum Hall effect and Berry's phase in graphene. *Nature* **2005**, *438*, 201–204.

[42] Faugeras, C.; Amado, M.; Kossacki, P.; Orlita, M.; Sprinkle, M.; Berger, C.; de Heer, W. A.; Potemski, M. Tuning the electron-phonon coupling in multilayer graphene with magnetic fields. *Phys. Rev. Lett.* **2009**, *103*, 186803.

[43] von Klitzing, K. The quantized Hall effect. *Rev. Mod. Phys.* **1986**, *58*, 519–531.

[44] Novoselov, K. S.; Geim, A. K.; Morozov, S. V.; Jiang, D.; Katsnelson, M. I.; Grigorieva, I. V.; Dubonos, S. V.; Firsov, A. A. Two-dimensional gas of massless Dirac fermions in graphene. *Nature* **2005**, *438*, 197–200.

[45] Kashuba, O.; Fal'ko, V. I. Interplay between uniaxial strain and magnetophonon resonance in graphene. *Phys. Rev. B* **2013**, *87*, 161404.

[46] Goler, S.; Yan, J.; Pellegrini, V.; Pinczuk, A. Raman spectroscopy of magneto-phonon resonances in graphene and graphite. *Solid State Commun.* **2012**, *152*, 1289–1293.

Table of contents

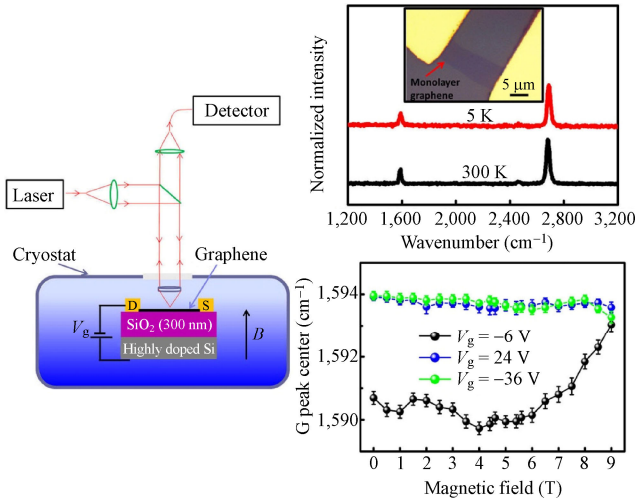

We report a study of the electrical field tuning of the magneto-phonon resonance in monolayer graphene by Raman spectroscopy.

Electronic Supplementary Material

Electrical field tuning of magneto-Raman scattering in monolayer graphene

Xiaonan Shen[1,§], Caiyu Qiu[1,2,§], Bingchen Cao[1], Chunxiao Cong[1], Weihuang Yang[1], Haomin Wang[1], and Ting Yu[1,3,4] (✉)

[1] *Division of Physics and Applied Physics, School of Physical and Mathematical Sciences, Nanyang Technological University, 637371 Singapore, Singapore*

[2] *Wenzhou Institute of Biomaterials and Engineering, Wenzhou 325001, China*

[3] *Department of Physics, Faculty of Science, National University of Singapore, 117542 Singapore, Singapore*

[4] *Graphene Research Center, Faculty of Science, National University of Singapore, 117546 Singapore, Singapore*

[§] *These authors contributed equally to this work.*

Supporting information to DOI 10.1007/s12274-014-0594-9

1 Calibration test for the custom designed magneto-Raman system

A commercial calibration grating sample [S1] (Anfatec-UMG02) was used to test our system. A SEM image of the calibration sample is shown in Fig. S1(a). The chess pattern structure makes it suitable for the lateral calibration. Confocal Rayleigh mapping images at room temperature and low temperature are shown in Figs. S1(b) and S1(c), respectively. From these test results, it is concluded that the spatial resolution can reach about 1 μm in our system.

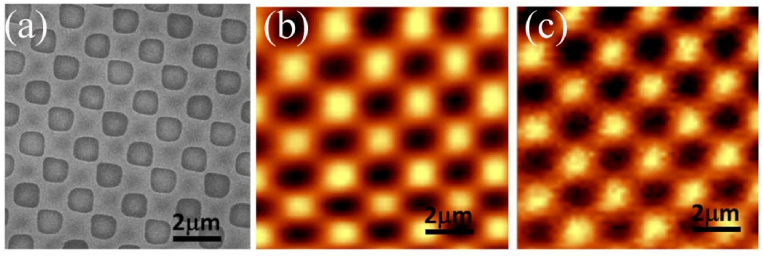

Figure S1 Calibration of our custom designed system. (a) SEM image of the sample which was used to calibrate our experimental setup. (b) Confocal mapping image of the calibration sample at room temperature (about 300 K). (c) Confocal mapping image of the calibration sample at low temperature (about 5 K).

2 Magneto-Raman scattering study on supported monolayer graphene

Magneto-Raman scattering experiments were carried out on several supported monolayer graphene samples. Exfoliated samples were prepared on top of the commonly used SiO_2 (300 nm)/Si substrate. An optical image of

Address correspondence to yuting@ntu.edu.sg

one representative graphene sample is shown in Fig. S2(a), where the monolayer region is indicated by the red arrow. Magnetic field dependent evolution of the G peak center and the FWHM for the monolayer graphene are shown in Fig. S2(b). This result is similar to that for the gated graphene when V_g is –6 V (as shown in Fig. 3). A possible reason for this is that this as-exfoliated sample is nearly intrinsic or not highly doped at low temperature in the vacuum environment.

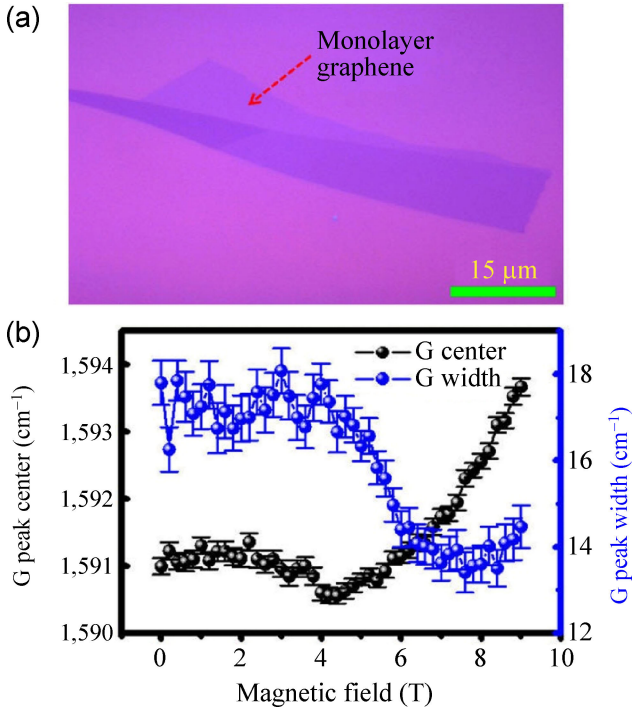

Figure S2 Magneto-Raman scattering in supported monolayer graphene. (a) Optical image of the as-exfoliated sample which contains monolayer graphene (indicated by the red arrow). (b) Evolution of the G peak center and the FWHM under magnetic fields for the monolayer graphene.

3 Simulation studies on the monolayer graphene

Based on the prediction by Ando [S2], an equation (Eq. (S1)) was developed in Potemski's work [S3] to analysis the magneto-phonon resonance in graphene. The same model was used here to extract the parameters

$$\tilde{\varepsilon}^2 - \varepsilon_0^2 = 2\varepsilon_0 \lambda E_1^2 \sum_{k=0}^{\infty} \left\{ \frac{T_k}{\left(\tilde{\varepsilon} + i\delta\right)^2 - T_k^2} + \frac{1}{T_k} \right\} \tag{S1}$$

$$\tilde{\varepsilon} = \varepsilon - i\Gamma \tag{S2}$$

$$T_k = (\sqrt{k} + \sqrt{k+1})E_1, E_1 = \sqrt{2e\hbar v_F^2 B}, (k = 0,1,2,\ldots) \tag{S3}$$

where ε_0 stands for the phonon energy at B = 0 T, ε and Γ stand for the energy and width of the G phonon under magnetic field, λ is the interaction strength between the G phonon and the magnetoexcitation, δ stands for the broadening of the magnetoexcitation, T_k denotes the energy of the magnetoexcitation and v_F represents the Fermi velocity.

Experimental data and simulation results are compared in Fig. 3. Extracted values are: the interaction strength $\lambda = 5 \times 10^{-3}$, the broadening factor $\delta = 400$ cm^{-1} = 49.6 meV, the phonon energy at zero magnetic

field $\varepsilon_0 = 1,586.6$ cm^{-1}, and the Fermi velocity $v_F = 1.21 \times 10^6$ m^2·s^{-1}. They are reasonable and comparable to previous results.

Although the detailed field dependent features such as the oscillations of both G peak center and FWHM found in the theoretical curves are not clearly reflected in the experimental data, the dominant feature near B = 3.5 T corresponding to the strongest MPR due to the $LL_{-2,1}^{-1,2}$ transition can be seen. The deviation between the theoretical and experimental data could be due to the relatively poor quality of the sample and/or the uniformly distributed non-intentional doping from the substrate.

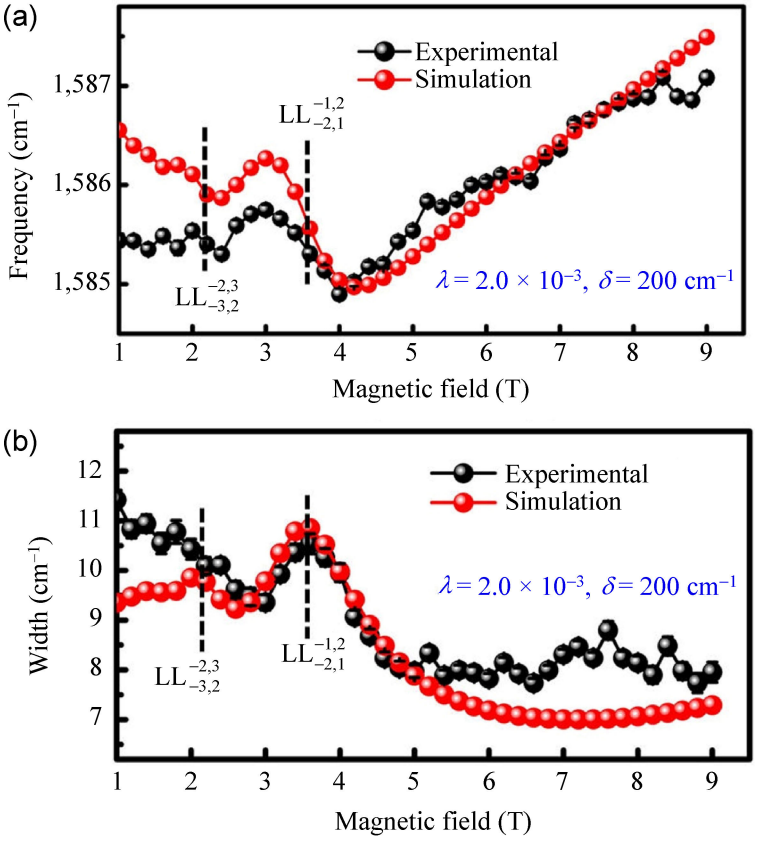

Figure S3 Simulation results compared with experimental data for the G peak center and the FWHM as a function of magnetic field for the exfoliated suspended monolayer graphene shown in Fig. 4. The parameters λ and δ used in the simulations are specified in the figures.

Experimental data and simulation results for the suspended monolayer graphene are compared in Fig. S3. Extracted values are: The interaction strength $\lambda = 2 \times 10^{-3}$, the broadening factor $\delta = 200$ cm^{-1} = 24.8 meV, the phonon energy at zero magnetic field $\varepsilon_0 = 1,585$ cm^{-1}, and the Fermi velocity $v_F = 1.21 \times 10^6$ m^2·s^{-1}. In addition to the main features, another small oscillation is also observed, which corresponds to the MPR caused by another transition between LLs as illustrated.

4 Mobility of the carriers in graphene devices

The mobility of the monolayer graphene device can be extracted using the following formula [S4]

$$R_{\text{Total}} = R_{\text{contact}} + \frac{L}{We\mu\sqrt{n_0^2 + n^2}}, \quad n = \frac{C\left|V_g - V_{\text{Driac}}\right|}{e}$$

where R_{Total} is the total resistance, L and W represent the length and width of the device, respectively, n denotes the carrier density and n_0 is the residual carrier concentration in the device, μ is the mobility of the device and $C = 1.15 \times 10^{-4}$ F is the capacitance of 300 nm SiO_2. The transport data measured from the studied device are shown in Fig. S4 and the electron and hole mobilities can be fitted to be about 9,490 and 8,050 $cm^2 \cdot V^{-1} \cdot s^{-1}$, respectively.

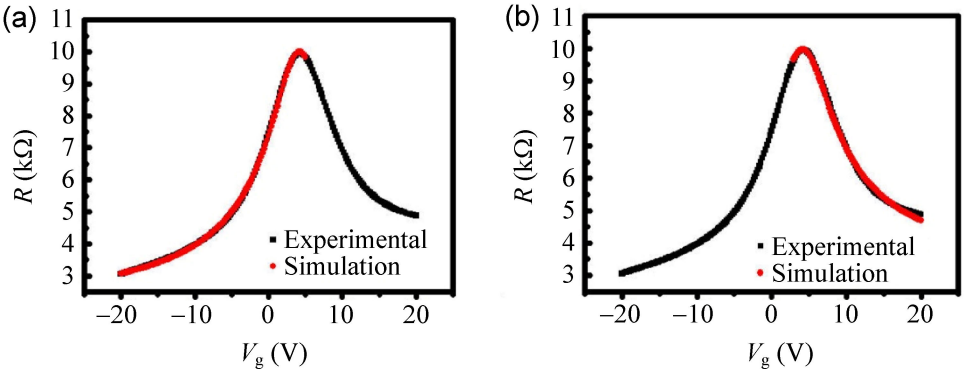

Figure S4 Simulation studies used to extract the values of the mobilities for (a) electrons and (b) holes.

5 Phonon anomaly in graphene devices

Ando's model was used to analyze the phonon anomaly phenomenon shown in Fig. 1(d). The formula we use (see below) is the same one as shown in Remi's work [S5]

$$\prod(\varepsilon_0) = \lambda\varepsilon_F - \frac{\lambda}{4}(\varepsilon_0 + i\delta)\left(\ln\left(\frac{\varepsilon_0 + 2\varepsilon_F + i\delta}{\varepsilon_0 - 2\varepsilon_F + i\delta}\right) + i\pi\right) \tag{S4}$$

$$\varepsilon_F = \hbar v_F \sqrt{\pi n} \tag{S5}$$

$$n = \frac{C\left|V_g - V_{Driac}\right|}{e} = 7.18 \times 10^{10} \frac{cm^{-2}}{V}\left|V_g - V_{Driac}\right| \tag{S6}$$

where, ε_0 stands for the phonon energy at $B = 0$ T, λ is the interaction strength, δ stands for the broadening factor, v_F represents the Fermi velocity, n means carrier concentration and ε_F is the Fermi level. The shift and broadening are given by the real and imaginary part of the Eq. (S4).

Substituting for values obtained from the MPR fitting (Fig. 3) into Eq. (S4) the interaction strength $\lambda = 5 \times 10^{-3}$, the broading factor $\delta = 49.6$ meV $= 400$ cm^{-1}, the phonon energy at zero magnetic field $\varepsilon_0 = 1{,}587.6$ cm^{-1}, the Fermi velocity $v_F = 1.21 \times 10^6$ $m^2 \cdot s^{-1}$, the phonon energies and the FWHMs for different back gates can be calculated. As shown in Fig. 1(d), good agreement between the simulated curves and the experimental data points is achieved.

6 Fano Resonance in graphene devices

The extracted asymmetry factors ($-1/q$) of our graphene device under various gates for $B = 0$ are provided and they are comparable to the previously reported values (see Fig. S5). Both sets of $-1/q$ data are within the range of 0.08 to 0, and vanish when the Fermi energy is large enough (~0.2 eV for both our sample and Yoon's sample) [S6].

Magnetic field induced modification of Fano resonances has been reported in previous studies of several materials like quantum wells, carbon nanotubes and topological materials [S7–S10]. Similar decreases of Fano resonances due to the presence of magnetic fields have also been experimentally observed in quasi-2D quantum wells [S7, S8]. The presence of the Fano resonances was confirmed by applying a magnetic field perpendicular to those quantum wells. Under various magnetic fields, the continuum of states in quantum wells splits into discrete excited excitonic states, thereby resulting in a progressively vanishing Fano resonance [S7].

As shown in the theory, the asymmetry factor $-1/q$ is proportional to the coupling strength between discrete states (G phonons here) and continuum states [S8]. When the magnetic field is applied perpendicular to graphene, the continuum band structure of graphene splits into discrete Landau levels. Thus, $-1/q$ decreases as B increases due to the weaker coupling.

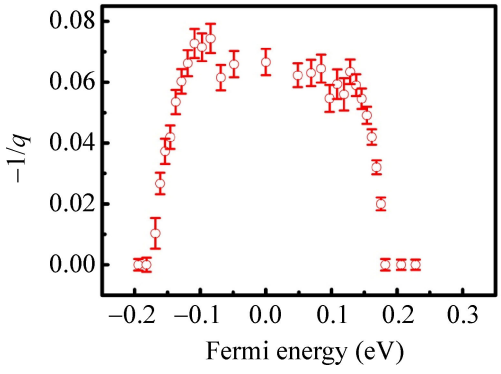

Figure S5 Asymmetry factor $-1/q$ as a function of the Fermi energy for graphene.

References

[S1] For detail information of the calibration sample, please visit this website: http://www.anfatec.de/mikromasch/umg02.html.

[S2] Ando, T. Magnetic Oscillation of Optical Phonon in Graphene. *J. Phys. Soc. Jpn.* **2007**, *76*, 024712.

[S3] Faugeras, C.; Amado, M.; Kossacki, P.; Orlita, M.; Sprinkle, M.; Berger, C.; de Heer, W. A.; Potemski, M. Tuning the Electron-Phonon Coupling in Multilayer Graphene with Magnetic Fields. *Phys. Rev. Lett.* **2009**, *103*, 186803.

[S4] Shen, X. N.; Wang, H. M.; Yu, T. How do the electron beam writing and metal deposition affect the properties of graphene during device fabrication? *Nanoscale* **2013**, *5*, 3352–3358.

[S5] Rémi, S.; Goldberg, B. B.; Swan, A. K. Charge Tuning of Nonresonant Magnetoexciton Phonon Interactions in Graphene. *Phys. Rev. Lett.* **2014**, *112*, 056803.

[S6] Yoon, D.; Jeong, D.; Lee, H. J.; Saito, R.; Son, Y. W.; Lee, H. C.; Cheong, H. Fano resonance in Raman scattering of graphene. *Carbon* **2013**, *61*, 373–378.

[S7] Oberli, D. Y.; Böhm, G.; Weimann, G.; Brum, J. A. Fano resonances in the excitation spectra of semiconductor quantum wells. *Phys. Rev. B* **1994**, *49*, 5757–5760.

[S8] Bellani, V.; Pérez, E.; Zimmermann, S.; Viña, L.; Hey, R.; Ploog, K. Evolution of Fano resonances in two- and three-dimensional semiconductors with a magnetic field. *Solid State Commun.* **1996**, *97*, 459–464.

[S9] Kim, J.; Kim, J. R.; Lee, J. O.; Park, J. W.; So, H. M.; Kim, N.; Kang, K.; Yoo, K. H.; Kim, J. J. Fano resonance in crossed carbon nanotubes. *Phys. Rev. Lett.* **2003**, *90*, 166403.

[S10] LaForge, A. D.; Frenzel, A.; Pursley, B. C.; Lin, T.; Liu, X. F.; Shi, J.; Basov, D. N. Optical characterization of Bi_2Se_3 in a magnetic field: Infrared evidence for magnetoelectric coupling in a topological insulator material. *Phys. Rev. B* **2010**, *81*, 125120.